Temperature-Responsive Separation Membrane with High Antifouling Performance For Efficient Separation

Tong Ji , Yuan Ji , Xiangli Meng * , Qi Wang

Posted Date: 4 January 2024

doi: 10.20944/preprints202401.0411.v1

Keywords: separation membranes; Temperature-responsive; PVDF; PVDF-g-NIPAAm; graphene oxide

Article

Temperature-Responsive Separation Membrane with High Antifouling Performance for Efficient Separation

Tong Ji †, Yuan Ji †, Xiangli Meng * and Qi Wang

[1] School of Chemistry and Chemical Engineering, Harbin Institute of Technology, 150001, Harbin 150001, PR China; 2247144927@qq.com (T.J.), jiyuan0713@163.com (Y.J.), wangqi_hit@sina.com (Q.W.)

* Correspondence: mengxl2009@hit.edu.cn

† These authors contributed equally to this work.

Abstract: Temperature-responsive separation membranes can significantly change their permeability and separation properties in response to changes in their surrounding temperature, improving efficiency and reducing membrane costs. This study focuses on the modification of commercial polyvinylidene fluoride (PVDF) membranes with amphiphilic temperature-responsive copolymer and inorganic nanoparticles. We prepared an amphiphilic temperature-responsive copolymer which the hydrophilic poly(N-isopropyl acrylamide) (PNIPAAm) was side-linked to a hydrophobic polyvinylidene fluoride (PVDF) skeleton. Subsequently, PVDF-g-NIPAAm polymer and graphene oxide (GO) blended with PVDF to prepare temperature-responsive separation membranes. The results showed that temperature-responsive polymers with different NIPAAm grafting ratios were successfully prepared by adjusting the material ratio of PVDF to NIPAAm. PVDF-g-NIPAAm was blended with PVDF with different grafting ratios to obtain separate membranes with different temperature responses. GO and PVDF-g-NIPAAm formed a relatively stable hydrogen bond network, which improved the internal structure and mechanical properties of the membrane without affecting the temperature response, thus extending the service life of the membrane.

Keywords: separation membrane; temperature-responsive; PVDF; PVDF-g-NIPAAm; graphene oxide

1. Introduction

The membrane is a versatile separation tool used in water purification, food purification, drug release, molecular separation, and molecular fractionation[1–3]. However, the balance between flux and selectivity is a major constraint for most conventional membranes[4,5]. New intelligence membrane material emerges to provide researchers with new insights[6,7].

In recent years, researchers have carried out smart separation membranes corresponding to different stimuli according to different fields, such as temperature[8], pH[9,10], pressure[11], light[12], electricity[13], magnetic field[14], and other responses[15,16]. This reduces the cost of membranes and extends the range of membrane applications[17]. To date, methods for the preparation of thermo-responsive ultrafiltration membranes generally involve involve blending or grafting modification of the thermal-responsive material with the membrane substrate polymer[18,19]. However, the current temperature-responsive membrane materials have a narrow adjustable range of response[20,21]. In particular, the introduction of thermo-responsive particles causes the internal structure of the membrane to become loose, which reduces the mechanical properties of the membrane and shortens its service life[1]. This is the reason why smart response functional separation membranes are not yet widely used.

In this study, an efficient separation membrane with temperature response was prepared by a submerged precipitation phase transformation method, using an amphiphilic temperature-responsive polymer and GO coblended with matrix PVDF. The temperature-responsive copolymer

 doi:10.20944/preprints202401.0411.v1

PVDF-g-PNIPAAm was prepared by grafting the PNIPAAm chain onto the PVDF backbone using an alkali treatment method. Afterward, PVDF was used as the base membrane material, GO and PVDF-g-PNIPAAm with different grafting ratios was blended with it to control the temperature-responsive effect of the PVDF/ PVDF-g-PNIPAAm/GO membrane.

2. Materials and Methods

2.1. Materials

PVDF was purchased from Shanghai Sanai Fuxin Material Co., Ltd. NIPAAm was obtained from Aladdin. Graphene oxide was purchased from Suzhou Hengqiu Technology Co., Ltd. *N*,*N*'-dimethylformamide (AR, DMF) and potassium hydroxide (KOH) was purchased from Tianjin Fengchuan Material Co., Ltd. Azodiisobutyronitrile (AIBN) was purchased from Beijing Bailingwei Technology Co., Ltd. polyvinylpyrrolidone (PVP, K30), absolute ethyl alcohol (99.5%) and *N*,*N*'-dimethylacetamide (AR, DMAC) were provided by Tianjin Damao Chemical Reagent Factory; BSA was purchased from Beijing Biological Technology Co., Ltd.,. These chemicals were used as received, LTD. All other reagents used in this work are commercially analytical grade and used without further purification.

2.2. Synthesis of PVDF-g-PNIPAAm polymer by alkali treatment

The PVDF powder was added into a 20wt% KOH alcohol solution (1:1 by the mass ratio of ethanol to water). The mass ratio of PVDF to KOH alcohol solution was 1:10. Subsequently, the PVDF powder was completely wetted by stirring, and the mixture was heated and stirred in a water bath at 60℃ for 30 min. After the solution was cooled, it was suction-filtered and washed 4 times with distilled water to remove KOH and ethanol from the surface. The product was dried in an oven at 60℃ for 24 h.

The alkali-treated PVDF powder (5.000 g) was added to 60 mL of DMF solvent, and the mixture was heated and stirred in a water bath at 60℃ to completely dissolve. NIPAAm monomer (2.500 g, 5.000 g, and 10.000 g) and initiator AIBN (0.084 g) were added and repeatedly vacuumed three times in a nitrogen atmosphere. Then, the mixture was stirred for 10 h in a water bath at 60℃ under a nitrogen atmosphere. After cooling to room temperature, the mixture was added a large amount of ethanol. The reaction product was washed repeatedly with distilled water more than 4 times to remove unreacted monomers and dry.

Three different PVDF-g-PNIPAAm polymers were prepared by controlling the mass ratio of PVDF to NIPAAM at the same reaction temperature, time, and initiator mass ratio. The mass ratios of PVDF to NIPAAM were 2:1, 1:1, and 1:2, respectively, and the corresponding products were named m21, m11, and m12, respectively.

2.3. Preparation of temperature-responsive Separation membrane

2.3.1. Preparation of PVDF/PVDF-g-PNIPAAm blending membrane

Pure PVDF, PVDF/PVDF-g-PNIPAAm blending membranes were prepared by immersion precipitation phase transformation method. DMAc was used as a solvent and PVP was used as a pore-making agent. The content of PVDF was 19.8 wt%, PVDF-g-PNIPAAm was 0.2 wt% and the content of PVP was 3.0 wt%. The weighed PVDF, PVDF-g-PNIPAAm, and PVP were added to DMAc, and the casting solution was prepared by stirring for 8 h at 60 °C. It was left to defoam for 24 h at room temperature. The cast membrane solution was poured onto a glass plate and scraped with a casting knife to make the membrane. Then, the glass plate with the casting solution was immersed in deionized water (30°C). The casting solution cures to form a membrane of appropriate size and thickness. Finally, the residual solvent was removed by thorough rinsing with deionized water. The membrane without PVDF-g-PNIPAAm was labeled as M0. The blended membranes containing PVDF-g-PNIPAAm numbered m21, m11, and m12 were labeled as M21, M11, and M12, respectively.

Preprints (www.preprints.org) | NOT PEER-REVIEWED | Posted: 4 January 2024 doi:10.20944/preprints202401.0411.v1

2.3.2. Preparation of PVDF/PVDF-g-PNIPAAm/GO separation membrane

The immobilized PVDF content was 19.8 wt%, the PVDF-g-PNIPAAm content was 0.2 wt%, and the PVP content was 3.0 wt%. DMAc was used as the solvent and the solidification bath temperature was 30 °C. The scheme design is shown in Table 1. GO was added to DMAc at ultrasonic for at least 5 h, which facilitated the dispersion of GO. PVDF, PVDF-g-PNIPAAm, and PVP were added to the dispersion and stirred in a water bath at 60 °C for 8 h. It was left to defoam for 24 h at room temperature. The casting solution was poured onto a glass plate and scraped with a casting knife to make the membrane. Then, the glass plate with the casting solution was immersed in deionized water (30°C). The casting solution cures to form a membrane of appropriate size and thickness. Finally, the residual solvent was removed by thorough rinsing with deionized water.

Table 1. Preparation process parameters of PVDF/PVDF-g-PNIPAAm/GO blending membrane.

Membranes	PVDF (wt%)	PVDF-g-PNIPAAm (wt%)	GO(wt%)
1	19.8	0.20	0.00
2	19.8	0.20	0.25
3	19.8	0.20	0.50
4	19.8	0.20	0.75
5	19.8	0.20	1.00

The formation process and temperature response behavior of PVDF/ PVDF-G-Pnipaam /GO films are shown in Scheme 1.

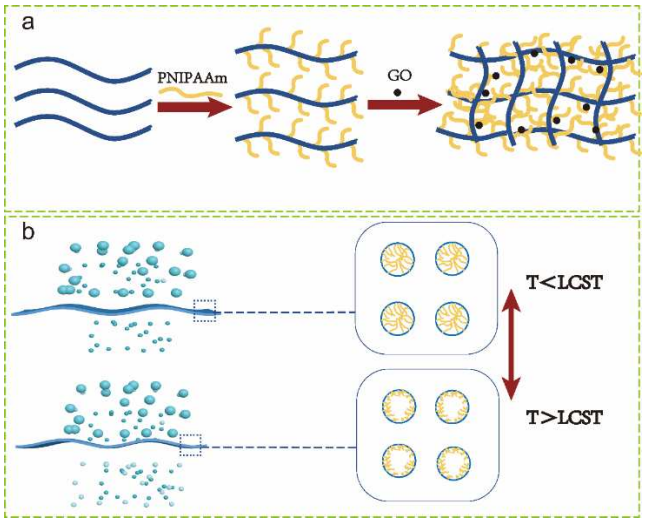

Scheme 1. a Schematic diagram of PVDF/PVDF-g-PNIPAAm/GO membrane formation; b Schematic illustration of temperature response behavior.

2.4. PVDF-g-PNIPAAm Characterization

The main functional group of the polymer was analyzed by a Nuclear magnetic resonance spectrometer(AVANCE III, Bruker). The grafting ratio of thermo-responsive polymers is calculated from the peak area of the proton characteristic peak. The grafting ratio is calculated as equation 1.

$$X = \frac{\frac{1}{6}A}{\frac{1}{2}(A_{hh}+A_{ht})+\frac{1}{6}A} \quad (1)$$

where X is the grafting ratio of PNIPAAm (%), A is the peak area of $CH(CH_3)_2$, A_{hh} is the peak area of hh ($-CF_2-CH_2-CH_2-CF_2-$) peak, and A_{ht} is the peak area of ht ($-CF_2-CH_2-CF_2-CH_2-$) peak.

The thermogravimetric method (TGA, SDT Q600) was used to analyze the thermal properties of the polymers. The sample was heated from Room temperature to 800°C at a rate of 10°C·min^{-1} under a dry nitrogen atmosphere.

2.5. Membrane Characterization

The mechanical properties of the membranes were measured using an electronic universal testing machine (Instron 5569, Instron, USA). The samples were measured at room temperature and 5 mm·min^{-1} of speed. Each group of samples was measured three times and averaged. The mechanical properties of the membrane were analyzed by comparing Young's modulus of the membrane.

The morphologies of membranes were observed by a scanning electron microscope (SEM, Instron 5569, Instron, America). To obtain the cross-section of the membrane, the membrane sample was fractured by immersing it in liquid nitrogen, then it was fixed on a sample stage sputtered with gold, and placed into the device for observation.

The surface hydrophilic property of a membrane was measured by a contact angle goniometer (POWER 2000) using the sessile drop method. At room temperature, a water droplet was dropped on the top surface, and the contact angle was recorded every 10 s. The reported data of contact angles were obtained by calculating the average of five repeated measurements.

2.6. Water Permeation Experiments

The pure water flux (Jw) of the ultrafiltration membrane refers to the volume of pure water permeating the membrane in a certain period over a unit membrane area under a certain filtration pressure.

In this experiment, the water flux of the membrane was measured by an MSC-300 cup ultrafilter. The ultrafiltration membrane was cut to a size suitable for the filter cup. The effective area of the membrane in this experiment was 36.32 cm^2. Before the test, the pressure was statically pressed at 0.1 MPa for 20 min. After the test solution was stabilized, the water flux of the membrane was measured under a pressure of 0.1 MPa, and the volume of water passing through a certain period was recorded to obtain a pure water flux. Water flux (Jw) was calculated by Equation (2):

$$J_w = \frac{V}{S \cdot t} \quad (2)$$

where J_w is the permeation flux of the membrane for pure water (L·h^{-1}·m^{-2}), V is the permeate liquid volume measured (L), *S* is the effective membrane area (m^2), and *t* is the permeation time (h).

2.7. Rejection property of the membrane

The rejection rate *R*(%) of the ultrafiltration membrane is indicative of the rejection effect of the ultrafiltration membrane on the bovine serum albumin solution under a certain pressure.

The permeate from the original solution after passing through the ultrafiltration membrane was collected at room temperature and a test pressure of 0.1 MPa. Finally, the absorbance of the original solution of BSA and the permeate at 280 nm was measured by an ultraviolet spectrophotometer. BSA protein rejection rate was calculated by Equation (3):

$$R = \left(1 - \frac{C_p}{C_f}\right) \times 100 \quad (3)$$

where *R* is the membrane rejection(%); C_f is the concentration of the original solution (mg·mL^{-1}); C_p is permeate concentration (mg·mL^{-1}).

2.8. Antifouling properties of the membrane

The anti-pollution performance of the ultrafiltration membrane is mainly measured by the water flux recovery rate *FRR* (%). The ultrafiltration membrane was tested according to the pure water flux test method described above and recorded as Jw1; then the same membrane was treated with

 doi:10.20944/preprints202401.0411.v1

ultrafiltration separation of bovine serum albumin solution for 30 min, and the ultrafiltration membrane then completely cleaned with distilled water. The membrane was again measured for pure water flux and recorded as Jw2. The anti-pollution performance of the ultrafiltration membrane was investigated by calculating the flux recovery rate from the ratio of the two. The flux recovery rate (FRR) was calculated by Equation (4):

$$FRR = \frac{J_{W1}}{J_{W2}} \times 100\% \quad (4)$$

Where J_{w1} is the pure water flux ($L \cdot h^{-1} \cdot m^{-2}$) before the use of the ultrafiltration membrane, J_{w2} is the pure water flux ($L \cdot h^{-1} \cdot m^{-2}$) after the use of the ultrafiltration membrane.

2.9. Porosity test of the membrane

The porosity of the membrane was obtained by the weighing method. The membrane was cut into squares of equal size. The mass of the membrane was weighed separately when dry and after immersion in pure water. The porosity is calculated as shown in Eq (5):

$$P_r = \frac{(W_W - W_d)}{S \cdot d \cdot \rho} \times 100\% \quad (5)$$

where W_w and W_d are the weight of the wet and dry membrane (g), S is the area of the measurement membrane (cm^2), d is the average thickness of the membrane (mm) and ρ is the density of distilled water at room temperature ($g \cdot cm^{-3}$).

3. Results and Discussion

3.1. Characterization of the synthesized PVDF-g-PNIPAAm graft polymers

In this study, PNIPAAm chains were branched onto the hydrophobic PVDF backbone by alkali treatment to prepare amphiphilic temperature responsive polymer, the mechanism of which is shown in Figure 1a. The reaction was carried out in two steps. The alkaline alcohol solution removes -F and -H from PVDF to form unsaturated bonds. Next, the initiator AIBN was employed to graft NIPAAM onto the PVDF backbone to form side chains. Three temperature-responsive polymers (m21, m11, and m12) with different NIPAAm grafting ratios were synthesized by adjusting the ratios of PVDF and NIPAAm mass. The 1H NMR spectra of PVDF-g-PNIPAAm showed new peaks at δ 1.1 ppm and 3.9 ppm, which were attributed to isopropyl and hypo methyl respectively, as shown in Fig 1b and 1c. In addition, the PNIPAAm grafting ratio of PVDF-g-PNIPAAm can be determined based on the ratio of (-CF_2-CH_2-CF_2-CH_2-, ht) and (-CF_2-CH_2-CH_2-CF_2-, hh) peak areas in the PVDF molecular chain with the isopropyl 1H NMR peak areas of PNIPAAm. The grafting ratios PVDF-g-PNIPAAm were calculated to be 4.9%, 8.3%, and 16.56%, respectively (Table 2).

Table 2. Grafting Rates of PNIPAAm in Polymers of Different Mass Ratios

number	The mass ratio of PVDF to NIPAAm	$X_{PNIPAAm}$(%)
m_{21}	2:1	4.9
m_{11}	1:1	8.3
m_{12}	1:2	16.56

In addition, the thermal stability of the polymers before and after the reaction was tested and the heat loss curves are shown in Fig 1d. The thermal weight loss curve of PVDF-g-PNIPAAm increased a thermal weight loss plateau (360°C) compared to the pure PVDF thermal weight loss curve, which was attributed to the disconnection of the side chain PNIPAAm. As can be seen, both 1H NMR and TG confirmed the successful preparation of PVDF-g-PNIPAAm polymer.

Preprints (www.preprints.org) | NOT PEER-REVIEWED | Posted: 4 January 2024 doi:10.20944/preprints202401.0411.v1

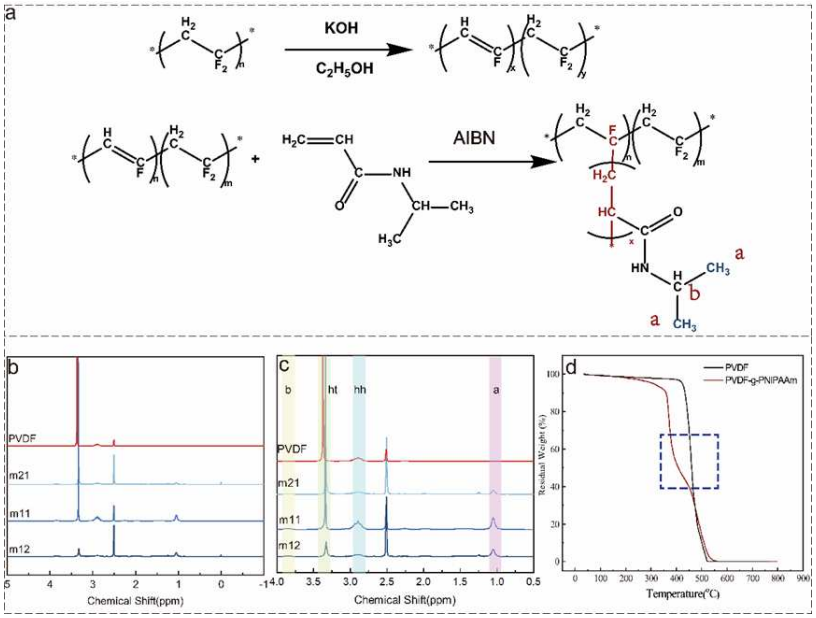

Figure 1. Reaction mechanism, NMR spectra, and TG curves of copolymer synthesis. (a) Reaction mechanism; (b) the full NMR spectrum of the copolymer; (c) the local spectrum of copolymer NMR; (d) TG curves of the copolymer.

3.2. Characterizations of PVDF/PVDF-g-PNIPAAm membrane

PVDF-g-PNIPAAm was blended with PVDF to prepare a temperature-responsive membrane. PVP was used as a pore-making agent. Water flux and rejection rates are indicators of membrane pore variation. In this study, the pure water flux and protein rejection of the PVDF/PVDF-g-PNIPAAm membrane were evaluated at different temperatures. The pure water fluxes of M21, M11 and M12 ranged from 500 to 901 $L \cdot m^{-2} \cdot h^{-1}$, 522 to 1032 $L \cdot m^{-2} \cdot h^{-1}$ and 604 to 1270 $L \cdot m^{-2} \cdot h^{-1}$ when the feed temperature was increased from 22°C to 40°C, respectively. In comparison, the pure water flux of the pure PVDF membrane (M0) ranged from 183 to 240 $L \cdot m^{-2} \cdot h^{-1}$ when the feed temperature was increased from 22 to 40 °C (Fig. 2a). It is clear that the pure water flux of the co-blended membrane increased with increasing temperature. the water flux of the membrane increases with the increase of temperature with the addition of temperature-responsive polymer.

We evaluated the temperature-responsive property of the membrane by the ratio of the water flux at 40°C and 22°C (J_{40}/J_{22}). The temperature response effect increases (J_{40}/J_{22}) from 1.802 to 2.103 with the increase of the polymer PNIPAAm grafting ratio(4.9% to 16.56%). When the permeate temperature is lower than LCST, the PNIPAAm chains stretch, Causing the membrane pores to shrink and even close; and when the permeate temperature is higher than LCST, the PNIPAAm chains contract, causing the membrane pores to be enlarged and the water flux is increased (Scheme 1). When the PNIPAAm grafting ratio increases, the water flux of the blended membrane becomes more temperature dependent, and thus the membrane becomes more thermo-responsive.

The rejection rate is an important indicator of membrane selectivity. Bovine serum protein was used as the standard rejection. As shown in Fig. 2b, the rejection of the blended membrane decreased when the PNIPAAm grafting ratio increased at the same temperature. This is because the PNIPAAm chains contain hydrophilic groups. The hydrophilic groups promote the exchange between solvent and non-solvent during the membrane-making process, leaving more holes in the interior of the membrane. When the temperature was increased from 22°C to 40°C, the rejection rates of membrane M21 and membrane M11 decreased with increasing temperature. This is due to the contraction of the branch chain of PNIPAAm, the increase of membrane pore size, and the decrease of the rejection rate due to the increase in temperature.

The M12 membrane has the opposite temperature-responsive behavior to the M21 and M11 membranes. This is due to the high PNIPAAm grafting ratio of the M12 membrane. When the

Preprints (www.preprints.org) | NOT PEER-REVIEWED | Posted: 4 January 2024 doi:10.20944/preprints202401.0411.v1

temperature is lower than LCST, the large pore size makes the BSA macromolecules pass through the membrane pores easily and the rejection rate is low despite the extended state of the PNIPAAm hydrophilic chain segments. Due to the high grafting ratio of PNIPAAm, the chain segments are entangled on the surface of the membrane and the surface of the membrane hole. When the temperature increases, the curling of the polymer chain does not increase the pore size of the membrane, and the entanglement of the side chain even blocks the pore of the membrane. Excessive entanglement of PNIPAAm side chains reduces the temperature sensitivity of the blend membrane.

Antifouling performance is a very important property of membranes, which determines the service life of the membrane. The membrane matrix material PVDF has strong hydrophobicity, which can easily adsorb retained materials and lead to contamination on the membrane surface and pore wall, and excessive contaminants lead to membrane pore blockage and membrane separation failure. As shown in Fig 2c, the antifouling ability of the separation membrane was also improved with the increase of the grafting rate of the temperature-responsive polymer. The increase in the PNIPAAm side chains promote the anti-fouling performance of the membrane. This is due to the hydrophilic groups in PNIPAAm inducing water molecules in the filtrate to form an aqueous layer on the membrane surface, which reduces the deposition of separates on the membrane surface. Meanwhile, the increase of membrane hydrophilicity reduces the adsorption of separates by the membrane.

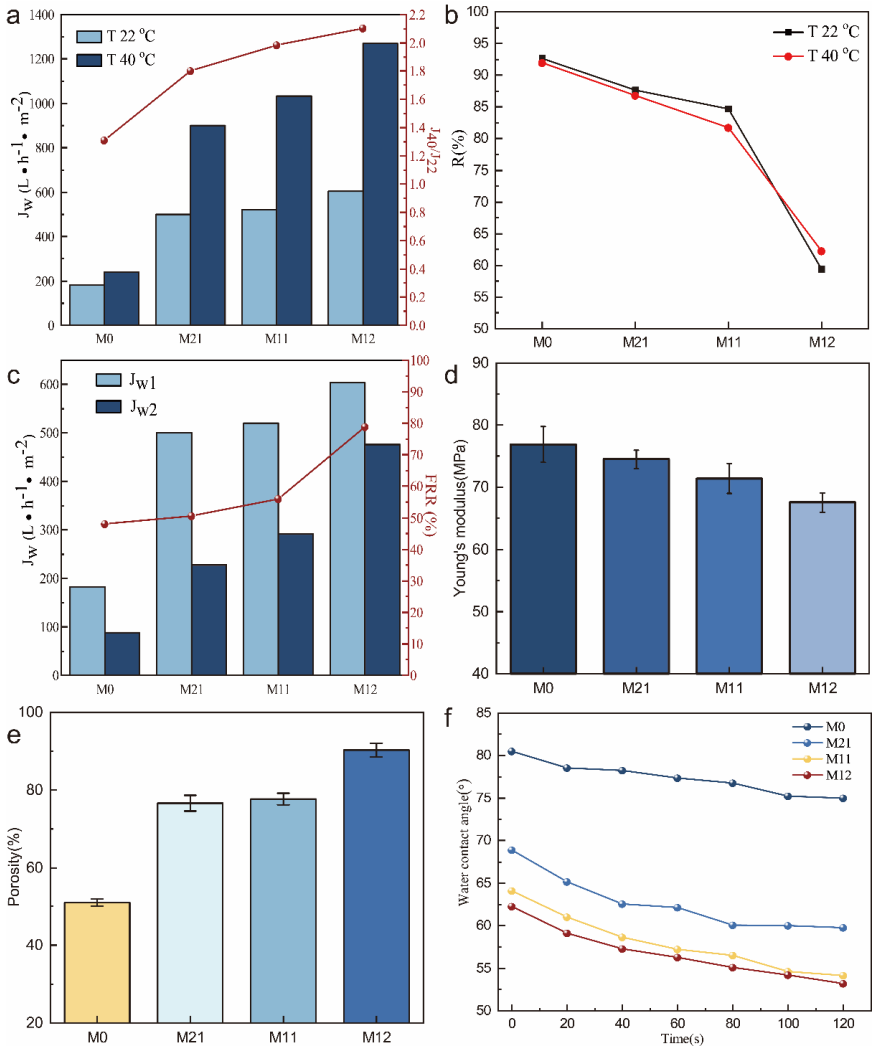

Figure 2. Comprehensive performance of PVDF/PVDF-g-PNIPAAm membranes (a) water flux (b) rejection rate (c) antifouling performance FRR (d) mechanical properties (e) porosity (f) water contact angle.

 doi:10.20944/preprints202401.0411.v1

To further analyze the structure of the temperature-responsive membrane, we characterized the porosity of the membranes. Figure 2e shows the porosity of the blended membranes with different NIPAAm grafting ratios. The PVDF membranes containing only the porogenic agent PVP had a lower porosity of 50.99%. The addition of the polymer significantly increased the porosity of the membrane. This may be attributed to the hydrophilic groups in the amphiphilic polymer inducing water molecules to enter the casting solution faster during the membrane curing process. This accelerated the exchange of solvent and nonsoluble components to create larger pores.

In addition, the surface hydrophilicity of the membrane was characterized by water droplet trapping (Fig. 2f). The 20s static water contact angle of the PVDF membrane without temperature-responsive polymer addition was 78.56°. The water contact angles of M21, M11 and M21 would be to 65.18°, 61.04° and 59.13°, respectively. In addition, the water contact angle of the pure PVDF membrane decreased from 80.51° to 75.01° at 120 s. While the water contact angle of the co-blended membrane decreased more obviously. After 120 s, the water contact angle of the M21 membrane decreased to 59.78°, the M11 membrane decreased to 54.14°, and the M12 membrane decreased to 53.17°. The results indicated that the hydrophilicity of the membranes increased with the increase in the PNIPAAm grafting ratio. This is consistent with the above characterization results.

However, we found that the addition of PVDF-g-PNIPAAm caused a decrease in the mechanical properties of the membranes. As shown in Figure 2d, Young's modulus of the blend membrane decreased with the increase of the PNIPAAm grafting ratio. It demonstrates that to the fact that the addition of PVDF-g-PNIPAAm increases the porosity of the membrane and the internal structure of the membrane becomes loose. It causes the membrane to reduce its ability to resist external forces. At the same time, It also explained that the rejection rate of the blend membrane decreases sharply when the grafting ratio of PNIPAAm is much too high.

This suggests that the temperature-responsive polymer has some improvement in the separation performance of the membrane while imparting a temperature-responsive function to the membrane. When the graft rate of PVDF-g-PNIPAAm was 8.3%, the temperature responsive property of the separation membrane was the best. However, the enhancement of the overall performance of the membrane has limitations.

3.1. Characterizations of PVDF/PVDF-g-PNIPAAm/GO membrane

In order to improve the overall performance of the membrane without affecting the temperature-responsive property. We considered introducing inorganic nanoparticles into the membrane. The PVDF-g-PNIPAAm and GO were added together into PVDF to prepare the PVDF/PVDF-g-PNIPAAm/GO separation membrane. Fig. 3 shows SEM photographs of different separation membranes, which include the upper surface and cross-section of the membrane. Figure 3a-3f showed PVDF/ PVDF-G-Pnipaam /GO membranes containing 0wt%, 0.25wt %, 0.50wt %, 0.75wt % and 1.00wt % GO, respectively. It is easy to find out that the incorporation of hydrophilic GO significantly changed the membrane pore structure. The surface of pure PVDF ultrafiltration membrane is smooth, and the number of pores is small and uniformly distributed. The addition of the PVDF-g-PNIPAAm increased the pore size of the membrane. However, it was still unevenly distributed, and the internal pores were mostly spongy. The addition of GO narrowed the pore size distribution on the membrane surface, and the membrane pores were more uniformly distributed and formed more finger-like pores inside.

Preprints (www.preprints.org) | NOT PEER-REVIEWED | Posted: 4 January 2024 doi:10.20944/preprints202401.0411.v1

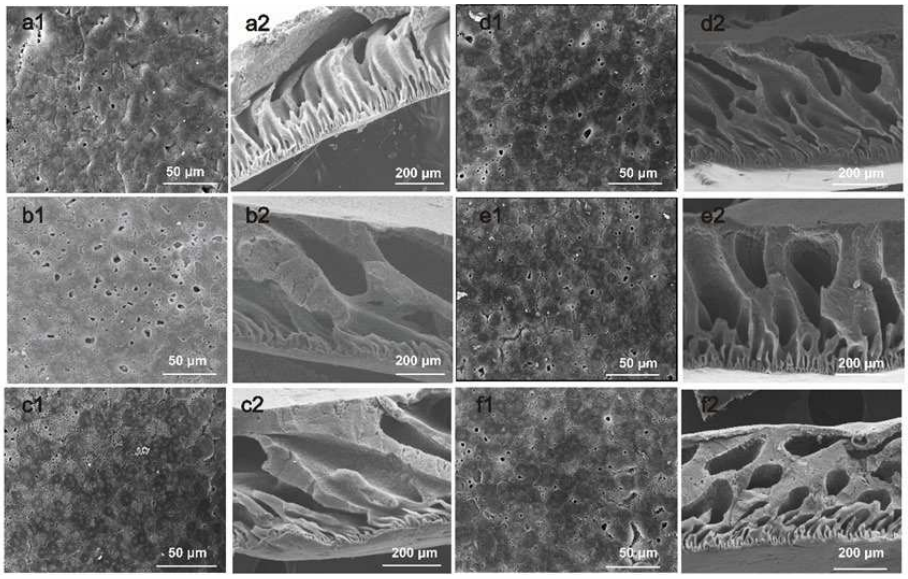

Figure 3. SEM photographs of the membranes. (a1-f1) The upper surfaces of pure PVDF membranes, PVDF/PVDF-g-PNIPAAm membranes, 0.25 wt%, 0.50 wt%, 0.75 wt%, 1.00 wt% GO content PVDF/PVDF-g-PNIPAAm/GO membranes. (a2-f2) The cross-section of the pure PVDF membranes, PVDF/PVDF-g-PNIPAAm membranes, 0.25 wt%, 0.50 wt%, 0.75 wt%, 1.00 wt% GO content PVDF/PVDF-g-PNIPAAm/GO membranes

Figure 4 shows the test results of hydrophilicity and porosity of the membranes. Figure 4a shows the hydrophilic characterization of the membrane after adding GO. We found that the addition of GO significantly improved the hydrophilicity of the membrane surface. Because graphene oxide is rich in hydrophilic groups. When the casting solution came into contact with water molecules, the GO attracted the water molecules, and eventually, the GO accumulated on the surface of the membrane. The amount and roughness of hydrophilic groups on the surface of the membrane were increased by graphene oxide, which improved the hydrophilicity of the membrane. However, in the characterization of membrane porosity, we found that the addition of GO containing rich hydrophilic groups caused the porosity of the membrane to decrease instead of increase (Figure 4b). According to the SEM photos, after GO was added, the inside of the membrane changed from large pores to more small pores (Figure 3). This is due to the fact that the hydrophilic groups on the GO surface and the PNIPAAm chains are connected by hydrogen bonds into a tighter network structure. The dense hydrogen bond network impedes the exchange rate between the water molecules entering the membrane and the solvent. It promotes the formation of uniform, small aperture finger pores.

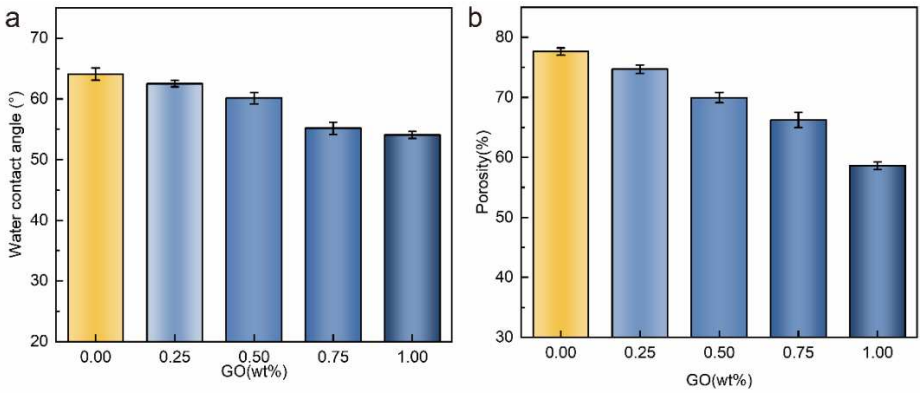

Figure 4. Porosity and hydrophilicity of PVDF/PVDF-g-PNIPAAm/GO membrane (a) Porosity (b) Hydrophilicity

Preprints (www.preprints.org) | NOT PEER-REVIEWED | Posted: 4 January 2024 doi:10.20944/preprints202401.0411.v1

We also used the ratio of water flux at 40°C and 22°C to evaluate the temperature-sensitive performance of the membrane. and the addition of graphene oxide has little effect on the temperature response of the membranes (Figure 5a). At the same time, the membrane rejection rate also increases with the addition of GO (Figure 5b). Combined with the membrane microstructure, we believe that the increase in the retention rate is due to the decrease in the number of large pore sizes and the decrease in the overall porosity, which restricts the passage of macromolecular proteins. In the anti-fouling test, it can be seen that the addition of GO significantly improves the anti-fouling performance of the membrane, as shown in Figure 5c. This is due to the increased hydrophilicity of the membrane surface, which reduces the deposition of contaminants on the membrane surface. In addition, the mechanical properties of the membranes were measured by tensile properties. The addition of GO increased Young's modulus of the membrane, which indicates that the structure of the membrane is tighter and can withstand more damage from external forces (Figure 5d). Overall, the addition of GO successfully achieved the anti-fouling and mechanical properties of the membrane. This is conducive to improving the service life of the membrane.

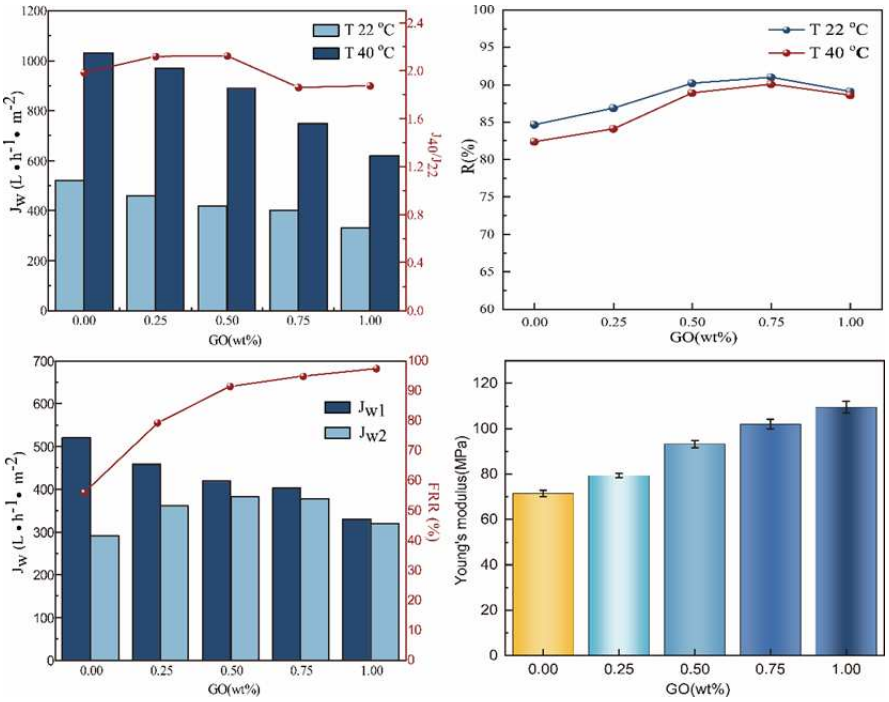

Figure 5. Comprehensive performance of PVDF/PVDF-g-PNIPAAm/GO membranes (a) water flux (b) rejection rate (c) antifouling performance FRR (d) mechanical properties

5. Conclusions

Temperature-responsive separation membranes have made great contributions to the field of water treatment. However, without affecting the temperature-sensitive properties of the membrane, it is very difficult to make it available for production applications. In this study, amphiphilic temperature-responsive polymers of different grafting ratios, PVDF-g-PNIPAAm, were successfully prepared. Subsequently, temperature-responsive separation membranes were prepared from these functional polymers. The temperature-responsive effect of the membrane was further enhanced by adjusting the PNIPAAm grafting ratio of the polymer. In addition, the pore structure on the membrane surface and inside was successfully improved by cross-linking hydrogen bonds between GO and PNIPAAm in the membrane. Thus, the membrane's separation effect and service life are improved without affecting the temperature response effect of the membrane. On the other hand, the formation of organic temperature-responsive polymers complemented with inorganic nanoparticles has great potential for fractionation.

Acknowledgments: This research did not receive any specific grant from funding agencies in the public, commercial, or not-for-profit sectors.

Conflicts of Interest: The authors declare no conflict of interest.

References

1. Liu, Z.; Wang, W.; Xie, R.; Ju, X.J.; Chu, L.Y. Stimuli-responsive smart gating membranes. *Chem Soc Rev* **2016**, *45*, 460-474, doi:10.1039/c5cs00692a.
2. Suwal, S.; Doyen, A.; Bazinet, L. Characterization of protein, peptide and amino acid fouling on ion-exchange and filtration membranes: Review of current and recently developed methods. *J Membrane Sci* **2015**, *496*, 267-283, doi:10.1016/j.memsci.2015.08.056.
3. Yusuf, A.; Sodiq, A.; Giwa, A.; Eke, J.; Pikuda, O.; De Luca, G.; Di Salvo, J.L.; Chakraborty, S. A review of emerging trends in membrane science and technology for sustainable water treatment. *J Clean Prod* **2020**, *266*, doi:ARTN 12186710.1016/j.jclepro.2020.121867.
4. Irfan, M.; Waqas, S.; Arshad, U.; Khan, J.A.; Legutko, S.; Kruszelnicka, I.; Ginter-Kramarczyk, D.; Rahman, S.; Skrzypczak, A. Response Surface Methodology and Artificial Neural Network Modelling of Membrane Rotating Biological Contactors for Wastewater Treatment. *Materials* **2022**, *15*, doi:ARTN 193210.3390/ma15051932.
5. Khorshidi, B.; Thundat, T.; Fleck, B.A.; Sadrzadeh, M. A Novel Approach Toward Fabrication of High Performance Thin Film Composite Polyamide Membranes. *Sci Rep-Uk* **2016**, *6*, doi:ARTN 22069 10.1038/srep22069.
6. Kim, H.S.; Park, S.J.; Nguyen, D.Q.; Bae, J.Y.; Bae, H.W.; Lee, H.; Lee, S.D.; Choi, D.K. Multi-functional zwitterionic compounds as new membrane materials for separating oletin-paraffin mixtures. *Green Chem* **2007**, *9*, 599-604, doi:10.1039/b614212e.
7. Sun, L.W.; Song, L.J.; Luan, S.F.; Yin, J.H. Progress in Photo-initiated Living Graft Polymerization of Biomaterials. *Acta Polym Sin* **2021**, *52*, 223-234, doi:10.11777/j.issn1000-3304.2020.20198.
8. Yin, B.B.; Wu, Y.N.; Liu, C.F.; Wang, P.; Wang, L.; Sun, G.X. An effective strategy for the preparation of a wide-temperature-range proton exchange membrane based on polybenzimidazoles and polyacrylamide hydrogels. *J Mater Chem A* **2021**, *9*, 3605-3615, doi:10.1039/d0ta08872b.
9. Diez-Pascual, A.M.; Shuttleworth, P.S. Layer-by-Layer Assembly of Biopolyelectrolytes onto Thermo/pH-Responsive Micro/Nano-Gels. *Materials* **2014**, *7*, 7472-7512, doi:10.3390/ma7117472.
10. Liu, H.W.; Yang, S.S.; Liu, Y.W.; Miao, M.J.; Zhao, Y.; Sotto, A.; Gao, C.J.; Shen, J.N. Fabricating a pH-responsive membrane through interfacial in-situ assembly of microgels for water gating and self-cleaning. *J Membrane Sci* **2019**, *579*, 230-239, doi:10.1016/j.memsci.2019.03.010.
11. Ni, X.Q.; Xing, X.; Deng, Y.F.; Li, Z. Applications of Stimuli-Responsive Hydrogels in Bone and Cartilage Regeneration. *Pharmaceutics* **2023**, *15*, doi:ARTN 98210.3390/pharmaceutics15030982.
12. Mahdavi, H.; Rezaei, M.; Ahmadian-Alam, L.; Amini, M.M. A novel ternary Pd-GO/N-doped TiO2 hierarchical visible-light sensitive photocatalyst for nanocomposite membrane. *Korean J Chem Eng* **2020**, *37*, 946-954, doi:10.1007/s11814-020-0533-2.
13. Wang, X.; Feng, M.; Liu, Y.; Deng, H.N.; Lu, J. Fabrication of graphene oxide blended polyethersulfone membranes via phase inversion assisted by electric field for improved separation and antifouling performance. *J Membrane Sci* **2019**, *577*, 41-50, doi:10.1016/j.memsci.2019.01.055.
14. Rybak, A.; Rybak, A.; Kaszuwara, W.; Nyc, M.; Auguscik, M. Metal substituted sulfonated poly(2,6-dimethyl-1,4-phenylene oxide) hybrid membranes with magnetic fillers for gas separation. *Sep Purif Technol* **2019**, *210*, 479-490, doi:10.1016/j.seppur.2018.08.032.
15. Chen, Q.M.; Yu, X.W.; Pei, Z.Q.; Yang, Y.; Wei, Y.; Ji, Y. Multi-stimuli responsive and multi-functional oligoaniline-modified vitrimers. *Chem Sci* **2017**, *8*, 724-733, doi:10.1039/c6sc02855a.
16. Okada, K.; Miura, Y.; Chiya, T.; Tokudome, Y.; Takahashi, M. Thermo-responsive wettability via surface roughness change on polymer-coated titanate nanorod brushes toward fast and multi-directional droplet transport. *Rsc Adv* **2020**, *10*, 28032-28036, doi:10.1039/d0ra05471b.
17. Ye, Q.S.; Wang, R.; Chen, C.; Chen, B.L.; Zhu, X.Y. High-Flux pH-Responsive Ultrafiltration Membrane for Efficient Nanoparticle Fractionation. *Acs Appl Mater Inter* **2021**, *13*, 56575-56583, doi:10.1021/acsami.1c16673.
18. Li, J.J.; Zhu, L.T.; Luo, Z.H. Electrospun fibrous membrane with enhanced swithchable oil/water wettability for oily water separation. *Chem Eng J* **2016**, *287*, 474-481, doi:10.1016/j.cej.2015.11.057.
19. Wu, L.; Li, C.R.; Tao, Z.; Wang, H.; Ran, J.; Bakangura, E.; Zhang, Z.H.; Xu, T.W. Anionic quaternary ammonium fluorous copolymers bearing thermo-responsive grafts for fuel cells. *Int J Hydrogen Energ* **2014**, *39*, 9387-9396, doi:10.1016/j.ijhydene.2014.04.070.

20. Pan, Y.Q.; He, L.; Ren, Y.S.; Wang, W.; Wang, T.H. Analysis of Influencing Factors on the Gas Separation Performance of Carbon Molecular Sieve Membrane Using Machine Learning Technique. *Membranes-Basel* **2022**, *12*, doi:ARTN 10010.3390/membranes12010100.
21. Plisko, T.V.; Bildyukevich, A.V.; Burts, K.S.; Hliavitskaya, T.A.; Penkova, A.V.; Ermakov, S.S.; Ulbricht, M. Modification of Polysulfone Ultrafiltration Membranes via Addition of Anionic Polyelectrolyte Based on Acrylamide and Sodium Acrylate to the Coagulation Bath to Improve Antifouling Performance in Water Treatment. *Membranes-Basel* **2020**, *10*, doi:ARTN 26410.3390/membranes10100264.